

RCCFormer: A Robust Crowd Counting Network Based on Transformer

Peng Liu^a, Heng-Chao Li^{a,*}, Sen Lei^a, Nanqing Liu^a, Bin Feng^b and Xiao Wu^c

^aSchool of Information Science and Technology, Southwest Jiaotong University, Chengdu 611756, China

^bSchool of Physical Education, Southwest Jiaotong University, Chengdu 611756, China

^cSchool of Computing and Artificial Intelligence, Southwest Jiaotong University, Chengdu 611756, China

ARTICLE INFO

Keywords:
Crowd Counting
Transformer
CNN
Scale-aware

ABSTRACT

Crowd counting, which is a key computer vision task, has emerged as a fundamental technology in crowd analysis and public safety management. However, challenges such as scale variations and complex backgrounds significantly impact the accuracy of crowd counting. To mitigate these issues, this paper proposes a robust Transformer-based crowd counting network, termed RCCFormer, specifically designed for background suppression and scale awareness. The proposed method incorporates a Multi-level Feature Fusion Module (MFFM), which meticulously integrates features extracted at diverse stages of the backbone architecture. It establishes a strong baseline capable of capturing intricate and comprehensive feature representations, surpassing traditional baselines. Furthermore, the introduced Detail-Embedded Attention Block (DEAB) captures contextual information and local details through global self-attention and local attention along with a learnable manner for efficient fusion. This enhances the model's ability to focus on foreground regions while effectively mitigating background noise interference. Additionally, we develop an Adaptive Scale-Aware Module (ASAM), with our novel Input-dependent Deformable Convolution (IDConv) as its fundamental building block. This module dynamically adapts to changes in head target shapes and scales, significantly improving the network's capability to accommodate large-scale variations. The effectiveness of the proposed method is validated on the ShanghaiTech Part_A and Part_B, NWPU-Crowd, and QNRF datasets. The results demonstrate that our RCCFormer achieves excellent performance across all four datasets, showcasing state-of-the-art outcomes. The code will be available at <https://github.com/lp-094/RCCFormer>.

1. Introduction

Crowd counting is a key and challenging task that employs vision-based methods to estimate the number of people in unconstrained scenarios. In recent years, due to rapid population growth, crowd counting has gained significant attention for its wide-ranging applications in public crowd monitoring[1], video surveillance[2] and traffic control[3]. With the development of vision methods, a considerable amount of research has been conducted [4, 5, 6].

Among these methods, transformer-based methods [6, 7] tend to perform better than CNN-based methods. However, the transformer backbone [8, 9] is still limited by extracting single-level features. Relying solely on high-level features can cause the network to lose many detailed characteristics such as accurate location information of crowds. To solve this issue, CCTrans [7] employs element-wise addition for multi-layer feature fusion, and PTCNet[10] utilizes a cascading approach. However, both methods overlook the inherent information discrepancy in these approaches. To this end, we construct a simple but effective method to utilize both high-level and low-level information fully. We use the features from the last three stages of the backbone, process them

* This work was supported in part by the National Natural Science Foundation of China under Grant 62271418, and in part by the Natural Science Foundation of Sichuan Province under Grant 2023NSFSC0030 and 2025ZNSFSC1154, and in part by the Postdoctoral Fellowship Program and China Postdoctoral Science Foundation under Grant Number BX20240291.

*Corresponding author

ORCID(s): 0009-0005-2577-7371 (P. Liu)



Figure 1: The effectiveness of strong baseline and typical crowd counting challenges: (1) **Strong Baseline:** (top) strong baseline significantly improves several datasets compared to the vanilla method. (2) **Large-scale Variation:** different heads pose substantial scale variations, with the largest being several times larger than the smallest (middle); (3) **Complex background:** billboards, cluttered backgrounds, and other distractions complicate the task of counting (bottom).

through a series of operations, and input them into the cross-attention for selective fusion. We refer to this approach as a Strong Baseline. From Fig. 1 (first row), it is evident that

the strong baseline significantly improves several datasets compared to the vanilla method. For specific details, please refer to the Sec. 3.1.

After obtaining a strong baseline, we can extract sufficiently robust features for subsequent processing. However, due to the counting task being affected by the imaging distance of the camera and complex backgrounds, the following issues still exist:

(1) Large scale variation. Scale variation is one of the main challenges in crowd counting. As shown in Fig. 1 (second row), it can be observed that heads closer to the camera display larger scales, while those farther away seem smaller. This notable scale disparity among different head instances presents a challenge in thoroughly exploring all scales. To mitigate this challenge, numerous methods involve designing CNN architectures that integrate multi-scale feature representations by fusing features from different layers[10], branches[11], or multi-columns[12, 13]. However, traditional CNNs have inherent drawbacks, such as fixed-size and limited receptive fields, which restrict their ability to explore large scales and weaken their capability to perceive shape variations. This leads to poor performance in scenarios with large-scale variation and a variety of head target alterations. Hence, modeling adaptive and large-scale perception becomes essential for adapting the rapid intra- and inter-image scale and shape variety.

(2) Confusion between foreground and background. Complex background also poses a significant challenge to accurate counting. As depicted in Fig.1 (third row), objects such as mannequins on billboards, and complex-colored garments may be mistakenly identified as heads. Many existing methods leverage CNN-based attention mechanisms, such as channel attention, spatial attention, and CBAM, to mitigate this issue. For instance, inspired by spatial attention mechanism, Sindagi et al.[14] developed a global attention module to focus on the channel dimension of feature maps, as well as a spatial attention module to suppress irrelevant features. Similarly, Wang et al. [15] proposed spatial attention branch and channel attention branch, effectively integrating them through dot-product operations. However, these methods still struggle to yield satisfactory results due to the independent weighting of channel/spatial locations and the lack of effective foreground object modeling. Transformers can mitigate this issue to some extent, as they can model global contextual dependencies, providing global information to explore the correlations between the foreground and background. However, they are limited in modeling local context, which contains the fine-grained features necessary for distinguishing between heads and complex backgrounds. Therefore, the effective integration of global and local features is particularly important.

Based on the preceding analysis, we further propose a robust crowd counting network (RCCFormer) based on the strong baseline. To mitigate the **confusion between foreground and background**, we propose a Detailed Embedding Attention Block to better extract human heads

from complex backgrounds. Specifically, we leverage self-attention to extract global contextual information and employ our local attention to mine local detailed information, followed by selective fusion in a learnable manner. Our local attention efficiently captures detailed information at minimal computational cost compared to self-attention. Moreover, unlike CNNs, it generates dynamic weights, enhancing adaptability and effectively bridging the semantic gap with Transformers [16]. In order to solve the **large-scale variation** issue, we introduce Input-dependent Deformable Convolution (IDConv) in our framework. IDConv adaptively learns deformation variables and weights for convolutions through feature learning. Compared to vanilla convolutions and deformable convolutions, IDConv better models scale and shape-varied head targets. Subsequently, we construct an Adaptive Scale-Aware Module using IDConvs with varying dilation rates to enhance the learning of large-scale feature representations.

In summary, the contributions of this paper are four-fold:

- We establish a strong baseline that uses a multi-level feature fusion module to integrate the features of multiple stages in the backbone. It achieves significantly better performance than the vanilla baseline.
- We introduce the detail-embedded attention block (DEAB), which incorporates local attention with dynamic attributes to bridge the semantic gap with global self-attention. Through a learnable manner, we seamlessly blend local detail information with global context information to adaptively suppress background noise.
- We construct an adaptive scale-aware module (ASAM) based on our proprietary Input-dependent Deformable Conv (IDConv), which can learn convolutional weight adjustments and shape variations simultaneously, leading to more effective modeling of geometric transformations. This module enables more effective capturing of multi-scale feature representations.
- Extensive experiments across four popular benchmarks including ShanghaiTech Part_A and Part_B, UCF-QNRF, and NWPU-Crowd, show that our proposed RCCFormer reaches new state-of-the-art results.

The remainder of this paper is organized as follows. Section 2 reviews some important works related to our RCCFormer. In Section 3, we describe the implementation details of our RCCFormer. Section 4 contains extensive experiments on various crowd counting datasets. In Section 5, we summarize the whole paper.

2. Related Work

2.1. Crowd Counting

Existing deep learning-based crowd counting approaches are mainly divided into three categories: detection, regression counting, and density estimation. The detection-based methods [17, 18] involve detecting bounding boxes around human heads in the image and calculating the number of boxes to obtain the counting result. However, its performance is seriously affected in occlusion and dense scenes. The regression-based methods [19, 20] do not need annotation information and directly obtain the counts. While these methods may be straightforward, their precision in counting leaves something to be desired. Density estimation is currently the most mainstream method [4, 21], where a density map is generated through the network, and the sum of density values is the final counting result. More recently, researchers have developed various techniques and models around density estimation to improve crowd counting performance, mainly including multi-scale models and attention models – whose details are described below:

Multi-scale Models: To enhance the network’s adaptation to scale variation, early research adopted a multi-column method [12, 13] that effectively merge multi-scale features through branches with different receptive fields. Some researchers designed pyramid structures to explore multi-scale features. Sindagi et al. [22] proposed a Context Pyramid Convolutional Neural Network (CP-CNN) to enhance counting performance by constructing global and local multi-scale contexts. SASNet [23] utilized a feature pyramid network to learn cross-scale and feature-level correlations. The final prediction is the weighted average of individual predictions from different levels. Additionally, using dilated convolutions with different dilation rates to construct multi-scale feature representations is also a commonly used method. STNet [24] leveraged dilated convolutions to construct a tree structure, enabling the hierarchical parsing of coarse-to-fine crowd regions. However, they lack the ability to adaptively perceive different scales.

Attention Models: The attention mechanism plays an important role in crowd counting research by allowing the network to focus on the most relevant information within the input. Designing an appropriate attention module can effectively improve the performance of crowd counting. [25] proposed an attention-injective deformable convolutional network, which incorporates an attention map generator to highlight foreground areas. CAFNet [26] designed a guidance attention fusion to compensate spatial information of low-level and high-level feature maps. Guo et al. [27] proposed a group channel attention and learnable graph attention to suppress the background noise.

Despite the significant progress that has been achieved with the aforementioned CNN-based multi-scale and attention methods, the limited receptive field of CNNs constrains their ability to capture global context in large-scale and complex scenes, impacting the accuracy of crowd counting. Transformer-based networks can mitigate this issue to some

extent, as they have the ability to model global contextual dependencies. Therefore, this paper primarily utilizes Transformers as the basic architecture.

2.2. Vision Transformer

Since Dosovitskiy et al. [8] first introduced the Transformer into the field of computer vision, a large number of Transformer-based methods have been developed for downstream tasks [28, 29, 30, 31, 32, 33]. Drawing inspiration from the feature pyramid architecture, Wang et al. [9] designed a multi-scale hierarchical Transformer structure for dense prediction tasks. Subsequently, they further developed PVTv2 [34] by employing overlapping patches and convolutional feedforward networks to handle images of arbitrary scales. The DETR series [28, 35, 36] used a CNN backbone for visual feature extraction followed by Transformers for object detection. Li et al. proposed SegFormer [37], a simple, efficient, and robust semantic segmentation method.

Several studies have integrated Transformer-based methods into the field of crowd counting. TransCrowd [38] is the earliest work that constructs the weakly supervised crowd counting from the perspective of sequence to counting. CCTrans [7] adopted a pyramid transformer as the backbone and designed a multi-scale regression head to alleviate scale variations. CTASNet [39] employed CNN to estimate low-density crowds, while leveraging Transformer for high-density crowds, and implemented an adaptive selection and fusion at the task level. Nevertheless, it failed to fully explore the deep intersections and fusion between these two architectures. Qian et al. [40] proposed a multi-scale Transformer and used a segmentation-based attention module to obtain fine-grained features. SAANet [41] designed a deformer backbone to extract the features, aggregates multi-level features by a deformable transformer encoder, and introduced a count query in a transformer decoder to re-calibrate the multi-level feature maps. Phan et al [21]. employed CNN and Transformer architectures as the foundational network structures to develop a crowd counting framework that integrates density estimation and object detection.

These Transformer-based methods employ self-attention mechanism to capture global dependencies. However, they often lack the ability to extract local detail information, which is crucial for accurately identifying targets within complex backgrounds. In contrast, our approach integrates global self-attention with CNN-based local attention, enabling the simultaneous modeling of both global and local dependencies. This dual-focus strategy effectively leverages global contextual information and local detail information, thereby significantly enhancing the ability to accurately discern targets in complex scenes.

2.3. Deformable Mechanism

Deformable convolution [42, 43] is an effective mechanism that dynamically adjusts the shape of the convolutional kernel to better adapt to the features of target regions, effectively capturing non-uniform features of the target. Some researchers have incorporated the concept of

deformable convolution into Transformer structures. Deformable DETR [35] is the first to introduce the deformable idea into the Transformer architecture. Li et al. [44] proposed a deformable attention mechanism to adaptively perceive spatial structures. Liu et al. [45] draw inspiration from the foundational principles of Transformer, introducing DCNv3, which achieves a new performance record on the COCO dataset. Concurrently, designing novel deformable convolutions based on the characteristics of the task is also a focal point of research. Qi et al. [46] designed dynamic snake convolution based on the characteristics of tubular structures to enhance the perception of elongated structures. Zhang et al. [47] analyzed the shape characteristics of human heads and proposed a Normed-Deformable Convolution. Zuo et al. [48] produced a deformable attention module that combines a sparse spatial sampling strategy with long-range relationship modeling capability. Hence, given the significant scale variations and continuous changes characteristic in crowd counting tasks, we propose an input-dependent deformable convolution. By simultaneously learning convolution kernel offsets and weights based on input features, this approach enhances the perception of scale-varying targets.

3. Methodology

In this section, we first introduce the strong baseline and then introduce the proposed RCCFormer and the loss function.

3.1. Strong Baseline

Most methods adopt the last layer of the backbone for subsequent feature extraction. Nevertheless, the features extracted by merely relying on the last layer are inadequate. Thus, the straightforward approach is to extract features from multiple stages of the backbone. Previous methods [7, 10] mainly employ concatenation or element-wise addition for fusion. As depicted in Fig. 2 (a), **Element-wise addition** implies aggregating by upsampling the deep features and adding pixel by pixel with the shallow features. While it can reduce complexity, it might fail to handle semantic discrepancies among features. **Concatenation** (see Fig. 2 (b)) indicates aggregating feature maps from different stages along the channel dimension. However, the simple concatenation method still cannot effectively fuse features selectively. To address the aforementioned issues, we propose a novel **Multi-level Feature Fusion Module** for fusing backbone features via the cross attention mechanism [49] (see Fig. 2 (c)). This operation assists the model in selectively and deliberately focusing on crucial information from different input features. Subsequently, we added it to the vanilla crowd counting network as a **Strong Baseline**. Then, we will introduce this module in detail.

To be specific, we first use concatenation and element-wise addition simultaneously for initial fusion and then introduce cross-attention [49] for fine fusion. As shown in Fig. 2 (c), for the output features $\{F_2, F_3, F_4\}$, the feature size is firstly unified to one-eighth of the input image resolution

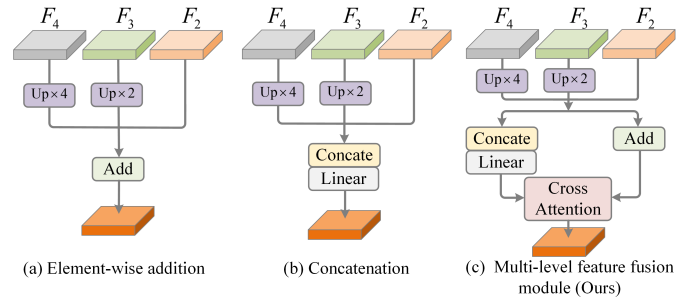


Figure 2: Different multi-level fusion methods. (a) element-wise addition; (b) concatenation; (c) our strong baseline.

Table 1

Comparison with the element-wise addition, concatenation and strong baseline on Part_A and UCFQNRf datasets.

Method	Part_A		QNRf	
	MAE	MSE	MAE	MSE
Element-wise addition	53.5	82.5	83.5	156.6
Concatenation	53.9	91.2	83.8	146.6
Strong baseline(Ours)	52.6	82.2	81.4	146.2

through the linear layer and upsampling layer, yielding features $\{F'_2, F'_3, F'_4\}$. In the concatenation branch, we employ concatenation and fuse different-level features using a linear layer to obtain F_c . In the addition branch, an element-wise addition is employed to obtain F_a . The detailed process is as follows:

$$\begin{aligned} F_c &= \text{Linear}(\text{Concat}(F'_2, F'_3, F'_4)) \\ F_a &= F'_2 + F'_3 + F'_4 \end{aligned} \quad (1)$$

where Concat is the concatenation and Linear denotes the linear layer. Then, the concatenated feature F_c is treated as query (Q), and the added feature F_a is regarded as key (K) and value (V). We leverage a cross-attention to interact with them and obtain the final fusion result, denoted as F_f .

$$F_f = \text{CrossAttn}(F_c, F_a, F_a) \quad (2)$$

where CrossAttn(\cdot, \cdot, \cdot) is the cross-attention.

We validated the effectiveness of our method on two crowd counting datasets named Part_A and UCF-QNRf. As shown in Table 1, our proposed strong baseline outperforms two traditional feature fusion methods, indicating that our approach extracts more robust features suitable for subsequent processing.

3.2. RCCFormer

Based on the Strong baseline, we further proposed RCCFormer. The overall framework of the proposed architecture is shown in Fig. 3. It consists of four main components: 1) Backbone network, where the Transformer network PVT-v2 is used to extract multi-level features $\{F_2, F_3, F_4\}$;

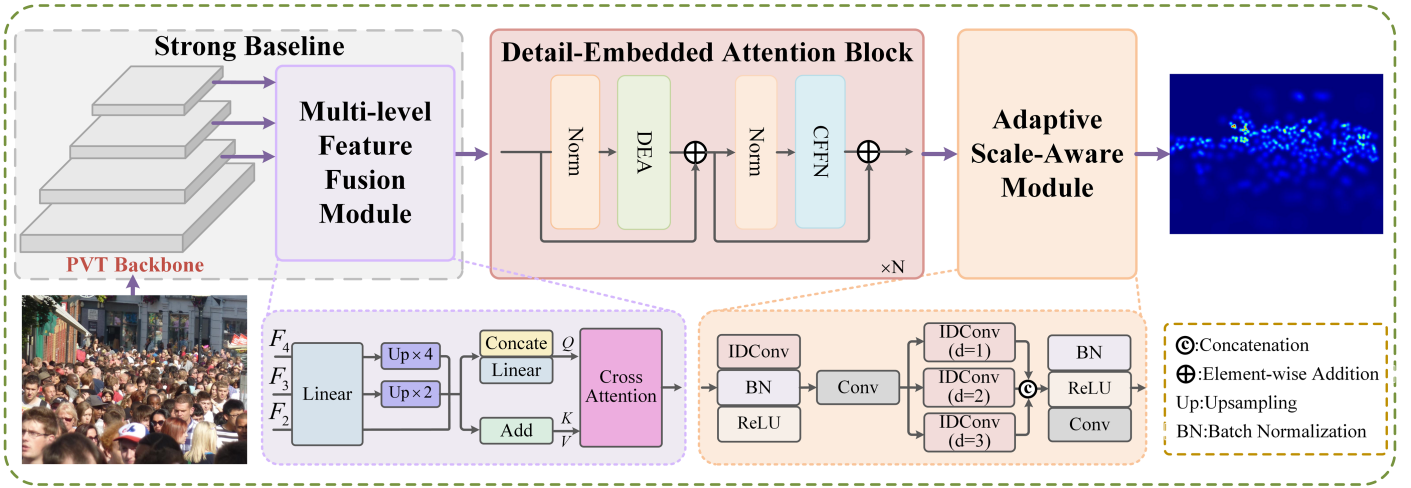


Figure 3: The overall framework of the proposed RCCFormer. It consists of three components: a strong baseline which contains pvt backbone and multi-level feature fusion module (MFFM), detail-embedded attention block (DEAB), and adaptive scale-aware module (ASAM). Among these, the MFFM integrates multi-level information; the DEAB extracts both global and local information for better suppression of background noise; the ASAM enhances the network's perceptual ability to large-scale variations. Some components are omitted for simplification. Please refer to the text for details.

2) **Multi-level Feature Fusion Module (MFFM)**, which utilizes concatenation, element-wise addition, and cross-attention to achieve better multi-level information fusion; 3) **Detail Embedded Attention Block (DEAB)**, which fully exploits global and local contextual information to amplify foreground targets and suppress background noise; 4) **Adaptive Scale-Aware Module (ASAM)**, where IDConvs with diverse dilation rates are employed to enhance the adaptive perception capability for large-scale objects. The details of DEAB and ASAM are described below.

3.2.1. Detail-Embedded Attention Block

When confronted with complex background challenges in crowded scenes, although Transformers can leverage self-attention mechanism to model global pixel-wise correlations, they lack positional awareness and fail to effectively attend to local details which are also important for understanding complex scenes. Therefore, we propose Detail-Embedded Attention Block (DEAB), an effective module for modeling global-local context information. Initially, through query (Q) and key (K) interactions, we obtain dependencies between global pixels and use it as global attention to perform matrix multiplication with value (V) to capture context information. Meanwhile, inspired by [50], we design local attention to extract local fine-grained representations. Specifically, a convolutional module with the local receptive field is employed to extract local dependencies, and its output is used as attention, which then performs element-wise multiplication with the V to generate the final output. In this way, the dynamic property can be obtained which is similar to those of the self-attention mechanism, effectively bridging the inherent semantic gap between CNNs and Transformers. Finally, the learnable manner is adopted to fuse the global and local context information selectively.

The overall structure of DEA is shown in Fig. 4. It can be seen that this module has two branches: the local attention branch and the global self-attention branch. For the global self-attention branch, given the input $X \in \mathbb{R}^{H \times W \times C}$, we reshape it into tokens $X_t \in \mathbb{R}^{HW \times C}$ and then project it into $Q \in \mathbb{R}^{HW \times C}$, $K \in \mathbb{R}^{HW \times C}$ and $V \in \mathbb{R}^{HW \times C}$:

$$Q = X_t W^Q, K = X_t W^K, V = X_t W^V \quad (3)$$

where W^K , W^V and $W^Q \in \mathbb{R}^{C \times C}$ are learnable projection matrixes. Subsequently, we split Q , K , and V into N heads along the channel dimension: $Q = [Q_1, \dots, Q_N]$, $K = [K_1, \dots, K_N]$, and $V = [V_1, \dots, V_N]$, respectively. The dimension of each head is $d_h = \frac{C}{N}$. Thus, for $head_j$, the self-attention is :

$$Attn_{ga_j} = \text{Softmax} \left(\frac{Q_j K_j^T}{\sqrt{d_h}} \right) \otimes V_j \quad (4)$$

For the local attention branch, given the same input $X \in \mathbb{R}^{H \times W \times C}$, we first feed it into 1×1 convolutional layer to projection. To better model the local detail information, we use one 5×5 depth-wise convolution to leverage local detail information and employ a 1×1 convolution to aggregate information across channels. Finally, to align with the multi-head features obtained from the global branch, we reshape the output features to $X \in \mathbb{R}^{N \times (H \times W) \times \frac{C}{N}}$. Similarly, for $head_j$, the local-attention is:

$$Attn_{la_j} = \text{Conv}_{1 \times 1} (\text{Conv}_{5 \times 5} (\text{Conv}_{1 \times 1})) \odot V_j \quad (5)$$

Finally, to enable the fusion of features in a learnable manner, we introduce a learnable parameter acting on local attention. So the output of the overall attention is:

$$Attn_j = Attn_{ga_j} + \alpha Attn_{la_j} \quad (6)$$

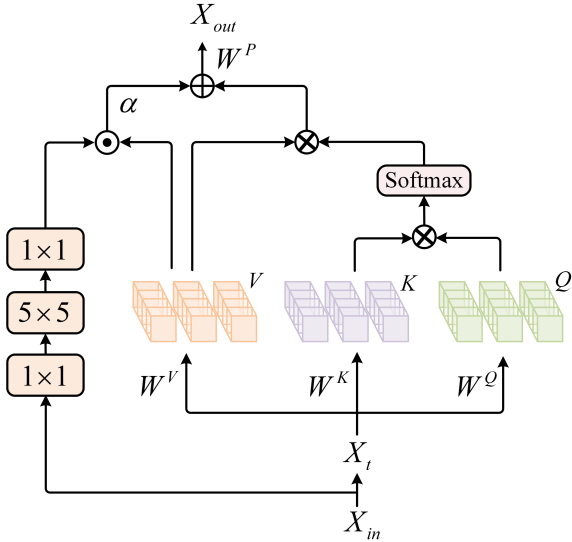


Figure 4: Illustration of the proposed Detail-Embedded Attention (DEA).

where α is a learnable parameter which is initialized to 0.6. Then, the detail-embedded attention is:

$$DEA = \text{Concat}(\text{Attn}_1, \dots, \text{Attn}_N)W^P \quad (7)$$

where W^P is also a learnable projection matrix.

After that, we use DEA as the core component and combine it with LayerNorm and convolutional feed-forward neural network (CFFN)[34] which is used to aggregate features to build a DEAB which is shown in the Fig. 3. This arrangement can be expressed as:

$$\begin{aligned} \hat{X} &= \text{DEA}(\text{LN}(X_{in})) + X_{in} \\ X_{out} &= \text{CFFN}(\text{LN}(\hat{X})) + \hat{X} \end{aligned} \quad (8)$$

where X_{in} is input feature, LN is layer normalization, and CFFN denotes the convolutional feed-forward neural network.

3.2.2. Adaptive Scale-Aware Module

In the previous discussion, the joint modeling of global and local dependencies has demonstrated its effectiveness in tackling complex background issues. However, the challenge of scale variation in crowd counting remains largely unresolved. Traditional methods frequently utilize convolutions with different kernel sizes, e.g., 3×3 , 5×5 , and 7×7 , or vary dilation rates to adapt to scale changes. Nonetheless, these methods are constrained by the fixed weights and sizes of convolutional kernels, limiting their adaptability to scale variations. Some others [11, 51] introduce deformable convolution and design adaptive dilation convolution to alleviate the shortcomings of vanilla convolution for crowd counting tasks, but only consider the geometric shape of the head and do not fully capture the head instance. To this end, we propose an input-dependent deformable convolution and

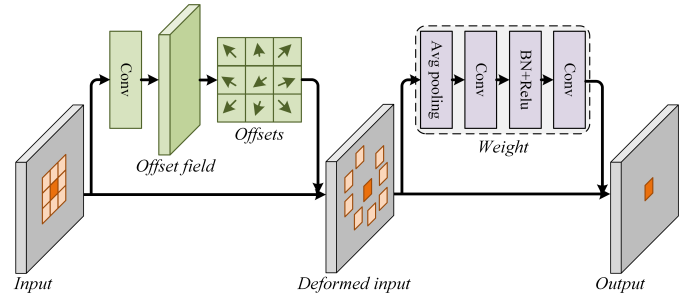


Figure 5: Illustration of the proposed Input-dependent Deformable Convolution.

build an adaptive scale-aware module, the details are as follows.

Input-dependent Deformable Convolution: inspired by the dynamic weight adjustment mechanism in self-attention, we propose an Input-Dependent Deformable Convolution named IDConv. This convolution adaptively learns the deformation parameters and weight coefficients of convolutional kernels, enabling these kernels to dynamically adjust their shapes and values in response to input data. This capability can provide strong robustness in crowd counting tasks, where the target scale and shape can vary significantly. Specifically, as illustrated in Fig. 5, our IDConv adaptively adjusts the offset of convolution sampling points and dynamically generates input-aware weights during the feature extraction process. Formally, the IDConv can be represented as

$$y(p_0) = \sum_{p_n \in R} w(p_n) \times x(p_0 + p_n + \Delta p_n) \quad (9)$$

where R represents the local receptive field, e.g., $R = (-1, -1), (-1, 0), \dots, (0, 1), (1, 1)$ when convolution kernel is 3×3 , p_0 denotes the central position of R , p_n represents the relative position of each value from R to p_0 , and $w(p_n)$ is a learnable weight, that is expressed as (10). Δp_n is a learnable offset which is generated by the 3×3 convolution, and define Δp_n as follows:

$$\begin{aligned} \Delta p_n &= \text{Conv}_{3 \times 3}(x) \\ w_{gap} &= \text{GAP}(x(p_0 + p_n + \Delta p_n)) \\ w(p_n) &= \text{Conv}_{1 \times 1}(\text{ReLU}(\text{BN}(\text{Conv}_{1 \times 1}(w_{gap})))) \end{aligned} \quad (10)$$

where $\text{Conv}_{3 \times 3}$ represents 3×3 convolution, $\text{Conv}_{1 \times 1}$ represents 1×1 convolution, BN is batch normalization, and ReLU is relu activation function. The GAP is a global average pooling operator.

Adaptive Scale-Aware Module: the IDConv is used as the basic component to build an adaptive scale-aware module as shown in Fig. 3. For the input feature $F_{in} \in \mathbb{R}^{H \times W \times C}$, we initially use a 3×3 IDConv with batch normalization and ReLU activation function to capture the local spatial information, and though 1×1 convolution to reduce channels to the half of the origin image, resulting in $F_m \in \mathbb{R}^{H \times W \times C}$.

Then, designing three parallel dilated IDConv operations, which dilations = $\{1, 2, 3\}$, to capture a large-scale range of the object. After that, the batch normalization and ReLU activation function are also used to provide normalization and nonlinearity, followed by a 1×1 convolution to obtain the output result $F_{out} \in \mathbb{R}^{H \times W \times C}$:

$$\begin{aligned} F_m &= \text{Conv}_{1 \times 1} \left(\text{ReLU} \left(\text{BN} \left(\text{IDConv}_{3 \times 3} (F_{in}) \right) \right) \right) \\ F_c &= \text{Concat} \left(\text{IDConv}_{3 \times 3, d} (F_m) \right)_{d \in \{1, 2, 3\}} \\ F_{out} &= \text{Conv}_{1 \times 1} \left(\text{ReLU} \left(\text{BN} (F_c) \right) \right) \end{aligned} \quad (11)$$

3.3. Loss Function

In our method, the loss function is based on DM-count [52] which considers crowd counting as a distribution matching problem and measures the similarity of the predicted density map and ground truth. Compared to traditional Gaussian density maps, this loss accurately captures real-world crowd distribution, particularly in dense regions. It consists of three components: the counting loss L_C , the optimal transport loss L_{OT} and the total variation loss L_{TV} , which are formulated as follows:

$$L_{count} = L_C(C', C) + \lambda_1 L_{OT}(D', D) + \lambda_2 L_{TV}(D', D) \quad (12)$$

where C' is the predicted count and C is ground truth count; D' and D represents the predicted density map and the ground truth. λ_1 and λ_2 are the weights of losses to realize a better mix of these losses which are set to 0.1 and 0.01, respectively.

4. Experiments

In this section, we first introduce the crowd counting dataset and experimental setting. Then, comparison experiments and ablation studies are carried out to verify the performance of our method.

4.1. Datasets

We conduct extensive experiments on four most commonly used crowd counting datasets: ShanghaiTech Part_A and Part_B [53], UCF-QNRF [54] and NWPU-Crowd [55], which are described as follows:

ShanghaiTech dataset consists of Part_A and Part_B, comprising a total of 1198 crowd images annotated by 330,165 people. Part_A includes 482 crowded internet images, with 300 images allocated for training and 182 for testing. Part_B consists of 716 sparse images captured at a fixed size of 768×1024 , with 400 images designated for training and 316 for testing.

UCF-QNRF dataset contains 1535 high-resolution images, with the number of people per image ranging from 49 to 12865, totaling 1,252,542 people. It owns the characteristics of diverse density, complex background, and distorted perspectives, which is extremely challenging.

NWPU-Crowd dataset is a large-scale dataset that consists of 5109 images, 3109 for training, 500 for validating, and 1500 for testing. The number of people in a single image ranges from 0 to 20033 in various diversity of scenes

with density variation and scale variation. In addition, 351 negative images are introduced to this dataset and it is more challenging for counting. According to density level, the testing set is divided into five fine-grained subsets, (1) S0: images of negative samples, (2) S1: images containing 1 ~ 100 people, (3) S2: images with 101 ~ 500 people, (4) S3: images with 501 ~ 5000 people and (5) S4: images contain more than 5000 people.

4.2. Experiment Settings

Implement details: Our approach adopts the backbone of PVTv2-B3 which is pre-trained on ImageNet-1K. For the data augmentation, we use random cropping and random horizontal flipping during the training stage. The image size is set to 512×512 for ShanghaiTech Part_B and QNRF dataset, and 384×384 for the NWPU-Crowd. As some images in ShanghaiTech Part_A are in low resolution, the size changes to 256×256 . Additionally, the batch size is 6 for all datasets, except for ShanghaiTech Part_A, which is set to 16. We adopt AdamW as the optimizer with the learning rate set to $1e^{-5}$ and weight decay set to $1e^{-4}$. All experiments are conducted on a single NVIDIA RTX4090 GPU using the PyTorch framework.

Evaluation Metrics: For the ShanghaiTech and QNRF datasets, we use Mean Absolute Error (MAE) and Mean Squared Error (MSE) as metrics to evaluate the performance of different methods. However, for the NWPU dataset, following [55], we have introduced the additional evaluation metric NAE (mean Normalized Absolute Error). These metrics are defined as follows:

$$MAE = \frac{1}{N} \sum_{i=1}^N |z_i - z_i^{gt}| \quad (13)$$

$$MSE = \sqrt{\frac{1}{N} \sum_{i=1}^N (z_i - z_i^{gt})^2} \quad (14)$$

$$NAE = \frac{1}{N} \sum_{i=1}^N \frac{|z_i - z_i^{gt}|}{z_i^{gt}} \quad (15)$$

where N is the number of test images, z_i and z_i^{gt} are the estimated number of people and the ground truth in the i -th images. It is noteworthy that the NWPU-Crowd has a number of negative samples with zero annotation, they are excluded during the calculation of NAE to avoid zero denominators.

4.3. Comparison with State-of-the-art Methods

We here conducted a series of qualitative experiments on these four datasets to verify the effectiveness of the proposed method. Notably, the majority of existing methods rely on CNN and Transformer architectures.

From Table 2, our model outperforms existing methods on the ShanghaiTech Part_A dataset, achieving the best

Table 2

Comparison with the state-of-the-art methods on Part_A, Part_B and UCF-QNRF datasets. The best results are highlighted in red, and the second-best results are highlighted in blue.

Method	Part_A		Part_B		UCF-QNRF	
	MAE ↓	MSE ↓	MAE ↓	MSE ↓	MAE ↓	MSE ↓
MCNN [53]	110.2	173.2	26.4	41.3	277.0	426.0
DM-Count [52]	59.7	95.7	7.4	11.8	85.6	148.3
P2PNet [56]	52.8	85.1	6.3	9.9	85.3	154.5
ChfL [57]	57.5	94.3	6.9	11.0	80.3	137.6
STNet [24]	52.8	83.6	6.2	10.3	87.9	166.4
GGANet [27]	62.0	110.7	7.4	13.1	91.9	156.8
CAAPN [58]	54.6	100.5	5.9	10.6	87.5	138.5
TransCrowd [38]	66.1	105.1	9.3	16.1	97.2	168.5
CCTrans [7]	52.3	84.9	6.2	9.9	82.8	142.3
CLTR [59]	56.9	95.2	6.5	10.6	87.3	142.4
CTASNet [39]	54.3	87.8	6.5	10.7	80.9	139.2
PET [60]	49.3	78.8	6.2	9.7	79.5	144.3
CF-former [61]	50.8	77.5	6.6	10.3	82.4	140.5
DEO-Net [21]	54.2	85.3	6.2	9.6	83.1	141.5
RCCFormer (Ours)	48.3	72.1	6.6	10.4	77.6	133.9

Table 3

Comparison with the state-of-the-art methods on NWPU-CROWD dataset. The best results are highlighted in red, and the second-best results are highlighted in blue.

Method	Overall			Scene Level(MAE)	
	MAE ↓	MSE ↓	NAE ↓	Avg. ↓	S0-S4 ↓
MCNN [53]	232.5	714.6	1.063	1171.9	356.0 / 72.1 / 103.5 / 509.5 / 4818.5
CSRNet [4]	121.3	387.8	0.604	522.7	176.0 / 35.8 / 59.8 / 285.8 / 2055.8
CAN [5]	106.3	386.5	0.295	612.2	82.6 / 14.7 / 46.6 / 269.7 / 2647.0
DM-Count [52]	88.4	388.6	0.169	498.0	146.7 / 7.6 / 31.2 / 228.7 / 2075.8
UOT [62]	87.8	387.5	0.185	566.5	80.7 / 7.9 / 36.3 / 212.0 / 2495.4
AutoScale [63]	94.2	388.2	0.226	608.2	81.4 / 11.4 / 38.2 / 226.1 / 2683.7
ChfL [57]	76.8	343.0	0.171	470.0	56.7 / 8.3 / 32.1 / 195.1 / 2058.0
CAAL [3]	76.4	327.4	0.182	470.0	27.9 / 8.2 / 37.3 / 189.7 / 2075.3
TransCrowd [38]	117.7	451.0	0.244	737.8	69.3 / 12.8 / 45.9 / 308.8 / 3252.2
MAN [6]	76.5	323.0	0.170	464.6	43.3 / 8.5 / 35.3 / 190.9 / 2044.9
CLTR [59]	74.4	333.8	0.165	423.3	4.2 / 7.3 / 30.3 / 185.5 / 2434.8
CTASNet [39]	94.4	357.6	0.213	497.3	52.1 / 10.4 / 42.5 / 264.1 / 2117.3
PET [60]	74.4	328.4	0.193	504.4	41.4 / 10.7 / 32.2 / 170.1 / 2267.9
RCCFormer (Ours)	74.3	332.7	0.160	401.0	82.2 / 6.9 / 29.9 / 201.8 / 1684.0

results with an MAE of 48.3 and MSE of 72.1. Compared to CNN-based methods, our model reduces MAE by 4.5 and MSE by 11.5 from the second-best result. Particularly, compared to existing Transformer-based approaches, our model reduces MAE by 1.0 and MSE by 5.4. For the ShanghaiTech Part_B dataset, our method shows a slight gap compared to the best result. The reason is the sparse distribution in this dataset, which results in heads occupying a relatively larger proportion of the images and containing significant detail information. This necessitates a heightened focus on

local features for accurate counting. However, our model is based on Transformer, which primarily focuses on global contextual information and only partially attends to local details, resulting in insufficient capture of the local features. On the UCF-QNRF dataset, our method also achieves the best result among the Transformer-based and CNN-based methods. Compared to the second-best result, our model shows a decrease of 1.9 in MAE and 3.7 in MSE, which demonstrates the enhanced performance of our model under large-scale variations and complex scenes.

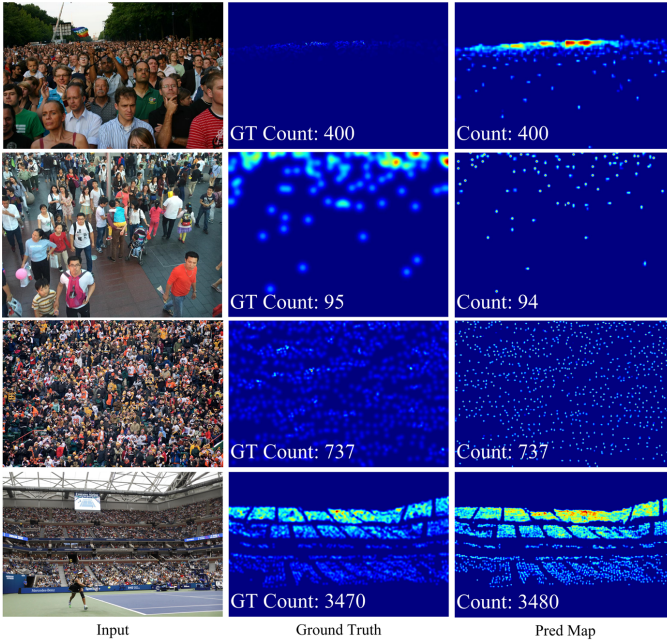


Figure 6: Visualization results on the four crowd-counting test datasets. From top to bottom, the images are from SHA, SHB, UCF-QNRF and NWPU-Crowd datasets, respectively.

To further investigate the performance of our RCCFormer on large-scale datasets, we conducted experiments on the NWPU-Crowd dataset. Compared to the previous three datasets, this dataset exhibits higher complexity in scene settings. The results in Table 3 demonstrate the effectiveness of our method. Our proposed RCCFormer achieves the best performance in MAE and NAE, with values of 74.3 and 0.160, respectively. However, because of the diversity in scene distribution within the NWPU dataset, the model cannot adapt well to all scenes, resulting in relatively high MSE. Notably, in the results for different density levels, it is observed that our model significantly outperforms previous methods on S4, which contains more than 5000 heads per image, indicating the superior performance of our model in high-density scenes.

The experimental analysis validates that our model excels in counting not only on sparse and simple images but also exhibits strong robustness in large-scale, complex crowd scenes. It effectively addresses the challenges posed by scale variations and complex background interference.

4.4. Visualization

We conduct visual analysis on four datasets: ShanghaiTech Part_A and Part_B, QNRF, and NWPU. Some results are shown in Fig. 6. The first row displays outcomes on ShanghaiTech Part_A images, showcasing the model’s robustness in achieving precise counting even in large-scale and densely populated scenes. The second row illustrates outcomes on ShanghaiTech Part_B images, verifying the model’s robust performance in sparse scenes. Results on QNRF, depicted in the third row, underscore the model’s

Table 4

Ablation studies of each component in our method based on the part_A dataset.

MFFM	DEAB	ASAM	MAE ↓	MSE ↓
			53.6	89.2
✓			52.6	82.2
✓	✓		50.0	79.9
✓	✓	✓	48.3	72.1

effectiveness in addressing the challenges presented by complex and varied backgrounds. Finally, the last row portrays outcomes on NWPU, demonstrating the model’s capability in both highly dense and complex scenes.

To further analyze the results with different methods, Fig. 7 presents visual comparisons of our RCCFormer with DM-Count [52] and CCTrans [7]. The examples include images with dense crowds and simple backgrounds (first row), highly crowded images (second row), images with large-scale variations (third row), and images with dense crowds and complex backgrounds (fourth row). It can be seen that the proposed RCCFormer consistently performs well in all these scenarios, producing density maps that are closest to the ground truth compared to the other two methods. Notably, when faced with significant background interference, as shown in the fourth row, the compared methods either overestimate or underestimate the crowd count, whereas our model’s predictions are close to the actual count. This demonstrates the robustness and effectiveness of our method.

4.5. Ablation Study

Effectiveness of Various Components. To validate the effectiveness of the designed modules including MFFM, DEAB, and ASAM, we conduct ablation experiments on the ShanghaiTech Part_A dataset, which the experimental results are shown in Table 4.

We upsample the final layer of the backbone to one-eighth of the image resolution and use a 1×1 convolution to output the density map as the baseline. From Table 4, it can be observed that, compared to the baseline, the introduction of the MFFM results in a decrease of 1.0 in MAE and 7.0 in MSE. This module can effectively integrate low-level fine-grained information and high-level semantic information, consequently providing more accurate positional cues for head instances. With the addition of the DEAB, the error further decreased, with MAE dropping to 50.0 and MSE decreasing to 79.9. It indicates that this block effectively achieves the separation of foreground and background, enhancing the extraction of foreground targets. Finally, with the implementation of the ASAM based on input-dependent deformable convolutions, MAE decreases by 1.7 and MSE decreases by 7.8, confirming the module’s ability to perceive a large-scale range and to effectively extract features from targets of various scales.

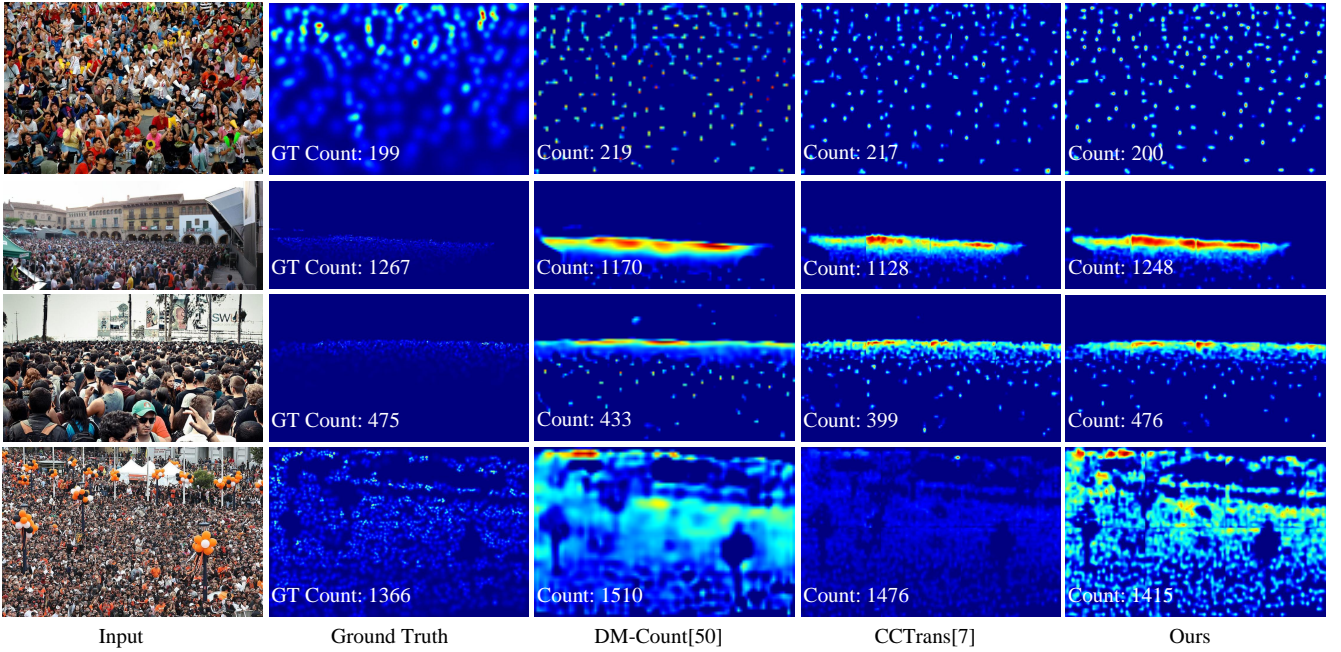


Figure 7: Visual comparison of predicted density maps generated by our method and DM-Count [52], CCTrans [7] under different scenes. It can be seen that our model consistently produces density maps closest to the ground truth.

Furthermore, we provide the illustration of density maps to visually analyze the impact of each module. Some visualization results are shown in Fig. 8, where Fig. 8 (a) depicts the input image with complex background and large-scale range, and Fig. 8 (b) represents the ground truth. Fig. 8 (c)-(f) respectively show the output density maps after the addition of the baseline, MFFM, DEAB, and ASAM. As depicted in Fig. 8 (d), compared to the baseline in Fig. 8 (c), the introduction of the MFFM enables more accurate localization of head targets. Additionally, as shown in Fig. 8 (a), the red box indicates background interference such as tree branches, and the density map in Fig. 8 (d) is affected by the tree branches. In contrast, Fig. 8 (e) and (f) is hardly influenced by the complex background, indicating that the DEAB effectively filters out background noise. Finally, within the green box in Fig. 8 (a) containing two human head targets of different scales, Fig. 8 (d) and (e) miss the smaller-scale target and the density value of another target is relatively low. However, Fig. 8 (f) successfully detects both targets, demonstrating that the addition of the ASAM enhances the network’s perception of target scales.

Effect of Multi-level Feature Fusion Module. To validate the effectiveness of our proposed MFFM, we compare five different fusion methods. Among them, Concat+Add+Concat initially merges multi-level information separately through concatenation and element-wise addition and then utilizes concatenation to fuse the information between them. Similarly, Concat+Add+Add does the same but utilizes element-wise addition to finally fuse the information between them. Compared to using only Concat and Add, our MFFM method reduces MAE by 1.3 and

Table 5

Ablation studies of different fusion methods.

Methods	MAE ↓	MSE ↓
Concat	53.9	91.2
Add	53.5	82.5
Concat+Add+Add	53.8	86.0
Concat+Add+Concat	52.8	83.9
MFFM (ours)	52.6	82.2

Table 6

Ablation studies of DEA.

Methods	MAE ↓	MSE ↓
GSA	51.3	81.7
GSA + Local Convolution	50.8	86.3
DEA (ours)	50.0	79.9

0.9, and MSE by 9 and 0.3, respectively. This indicates that further fusing the information between concatenation and element-wise addition using cross-attention can yield better multi-level fusion information. In comparison to Concat+Add+Concat and Concat+Add+Add, the experimental results of our MFFM method surpass both, demonstrating that cross-attention is a superior fusion method compared to Concat and Add.

Effect of Detail Embedded Attention Block. We compare the global self-attention (GSA), the global self-attention with integrated local convolutions, and the proposed DEA.

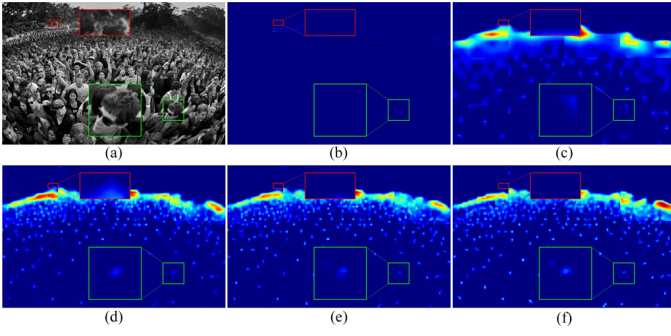


Figure 8: Examples of visualizations of the different modules. (a) Input Image. (b) Ground Truth. (c) Baseline. (d) Baseline + MFFM. (e) Baseline + MFFM + DEAB. (f) Baseline + MFFM+DEAB + ASAM.

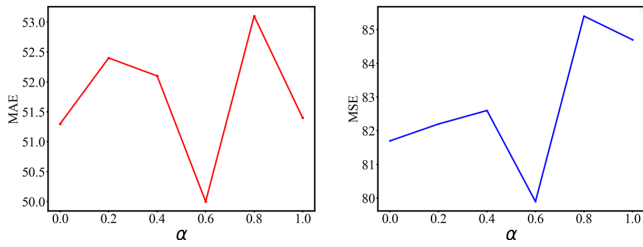


Figure 9: Effect of the value of the learnable parameter α .

Table 7

Ablation studies of the different convolution.

Methods	MAE ↓	MSE ↓
3×3 Convolution	51.5	79.2
5×5 Convolution	50.0	79.9
7×7 Convolution	52.7	86.7

As presented in Table 6, compared to the global self-attention, DEA showed a 0.7 improvement in MAE and a reduction of 1.8 in MSE. Furthermore, DEA outperforms global self-attention with integrated local convolutions, reducing MAE by 0.8 and MSE by 6.4. These findings underscore the effectiveness of embedding local information into global contexts in a learnable manner, facilitating superior extraction of valuable foreground information from intricate scenes.

Effect of Learnable Parameter α . We analyze the initialization values of the learnable parameter α in the DEAB. Through comparative experiments, we uniformly sampled six initial values from the range $[0, 1]$ and assessed their effects on counting performance. As depicted in Fig. 9, initializing α to 0.6 results in the minimum values for both MAE and MSE. Therefore, we set the initialization value of α to 0.6 in this paper.

Effect of Convolutions with Different Sizes. We delve into the impact of employing convolutions of different sizes

Table 8

Ablation studies of Input-dependent Deformable Conv.

Methods	MAE ↓	MSE ↓
Convolution	50.8	78.0
Deformable Convolution	51.3	77.9
IDConv (ours)	48.3	72.1

on counting performance within Detail-Embedded Attention. As detailed in Table 7, we compare convolutions sized 3×3 , 5×5 , and 7×7 . Interestingly, while the employment of a 5×5 convolution led to a slightly higher MSE compared to the 3×3 convolution, it results in the lowest MAE, outperforming the second-best result by 1.5 points. This highlights the advantage of utilizing a 5×5 convolution for extracting local detail information.

Effect of Input-dependent Deformable Convolution.

In the ASAM, we compare the effects of vanilla convolution, deformable convolution, and our input-dependent deformable convolution, as shown in Table 8. Overall, compared to vanilla convolution, IDConv reduces MAE and MSE by 2.5 and 5.9, respectively. MAE decreases by 5.8%, and MSE decreases by 7.4% than deformable convolution. This indicates that dynamically changing the convolutional kernel weights and shapes based on the input features is more conducive to improving crowd counting performance.

5. Conclusion

In this paper, we propose RCCFormer, a novel Transformer-based model designed to address the challenges of scale variation and background interference in crowd counting. Our approach leverages an innovative local-global attention block to extract both local and global contextual information, effectively mitigating the impact of complex backgrounds. Additionally, the adaptive scale-aware module is designed to provide adaptive perception abilities across varying head scales. Extensive experiments conducted on four popular crowd counting datasets, along with a visual analysis on the Shanghai Tech_A dataset, validate the efficacy of each module and highlight the superior performance of RCCFormer. Notably, our work shows that input-dependent deformable convolution is highly effective for scale-adaptive perception. In future work, we will focus on the challenge of missing labels in crowd counting tasks, particularly concentrating on unsupervised and semi-supervised learning. Our objective is to develop advanced methods capable of automatically extracting features from unlabeled data, thereby ensuring accurate and dependable crowd counting.

References

- [1] Jun Luo, Jinqiao Wang, Huazhong Xu, and Hanqing Lu. Real-time people counting for indoor scenes. *Signal Processing*, 124:27–35, 2016. Big Data Meets Multimedia Analytics.
- [2] Yingjie Xia, Xingmin Shi, Guanghua Song, Qiaolei Geng, and Yuncai Liu. Towards improving quality of video-based vehicle counting

- method for traffic flow estimation. *Signal Processing*, 120:672–681, 2016.
- [3] Yanda Meng, Joshua Bridge, Yitian Zhao, Martha Joddrell, Yihong Qiao, Xiaoyun Yang, Xiaowei Huang, and Yalin Zheng. Transportation object counting with graph-based adaptive auxiliary learning. *IEEE Transactions on Intelligent Transportation Systems*, 24(3):3422–3437, 2023.
- [4] Yuhong Li, Xiaofan Zhang, and Deming Chen. CSRNet: Dilated convolutional neural networks for understanding the highly congested scenes. In *2018 IEEE/CVF Conference on Computer Vision and Pattern Recognition*, pages 1091–1100, 2018.
- [5] Weizhe Liu, Mathieu Salzmann, and Pascal Fua. Context-aware crowd counting. In *Proceedings of the IEEE/CVF Conference on Computer Vision and Pattern Recognition*, pages 5099–5108, 2019.
- [6] Hui Lin, Zhiheng Ma, Rongrong Ji, Yaowei Wang, and Xiaopeng Hong. Boosting crowd counting via multifaceted attention. In *Proceedings of the IEEE/CVF Conference on Computer Vision and Pattern Recognition*, pages 19628–19637, 2022.
- [7] Ye Tian, Xiangxiang Chu, and Hongpeng Wang. CCTrans: Simplifying and improving crowd counting with transformer. *arXiv preprint arXiv:2109.14483*, 2021.
- [8] Alexey Dosovitskiy, Lucas Beyer, Alexander Kolesnikov, Dirk Weissenborn, Xiaohua Zhai, Thomas Unterthiner, Mostafa Dehghani, Matthias Minderer, Georg Heigold, Sylvain Gelly, et al. An image is worth 16x16 words: Transformers for image recognition at scale. *arXiv preprint arXiv:2010.11929*, 2020.
- [9] Wenhai Wang, Enze Xie, Xiang Li, Deng-Ping Fan, Kaitao Song, Ding Liang, Tong Lu, Ping Luo, and Ling Shao. Pyramid vision transformer: A versatile backbone for dense prediction without convolutions. In *Proceedings of the IEEE/CVF International Conference on Computer Vision*, pages 568–578, 2021.
- [10] Jiayu Liu, He Li, and Weihang Kong. Multi-level learning counting via pyramid vision transformer and cnn. *Engineering Applications of Artificial Intelligence*, 123:106184, 2023.
- [11] Shuai Bai, Zhiqun He, Yu Qiao, Hanzhe Hu, Wei Wu, and Junjie Yan. Adaptive dilated network with self-correction supervision for counting. In *Proceedings of the IEEE/CVF Conference on Computer Vision and Pattern Recognition*, pages 4594–4603, 2020.
- [12] Yanbo Liu, Guo Cao, Hao Shi, and Yingxiang Hu. Lw-Count: An effective lightweight encoding-decoding crowd counting network. *IEEE Transactions on Circuits and Systems for Video Technology*, 32(10):6821–6834, 2022.
- [13] Biao Yang, Weiqin Zhan, Nan Wang, Xiaofeng Liu, and Jidong Lv. Counting crowds using a scale-distribution-aware network and adaptive human-shaped kernel. *Neurocomputing*, 390:207–216, 2020.
- [14] Vishwanath A Sindagi and Vishal M Patel. HA-CNN: Hierarchical attention-based crowd counting network. *IEEE Transactions on Image Processing*, 29:323–335, 2019.
- [15] Shunzhou Wang, Yao Lu, Tianfei Zhou, Huijun Di, Lihua Lu, and Lin Zhang. SCLNet: Spatial context learning network for congested crowd counting. *Neurocomputing*, 404:227–239, 2020.
- [16] Qi Han, Zejia Fan, Qi Dai, Lei Sun, Ming-Ming Cheng, Jiaying Liu, and Jingdong Wang. On the connection between local attention and dynamic depth-wise convolution. *arXiv preprint arXiv:2106.04263*, 2021.
- [17] Yuting Liu, Miaojing Shi, Qijun Zhao, and Xiaofang Wang. Point in, box out: Beyond counting persons in crowds. In *Proceedings of the IEEE/CVF Conference on Computer Vision and Pattern Recognition*, pages 6469–6478, 2019.
- [18] Yi Wang, Junhui Hou, Xinyu Hou, and Lap-Pui Chau. A self-training approach for point-supervised object detection and counting in crowds. *IEEE Transactions on Image Processing*, 30:2876–2887, 2021.
- [19] Ke Chen, Shaogang Gong, Tao Xiang, and Chen Change Loy. Cumulative attribute space for age and crowd density estimation. In *Proceedings of the IEEE/CVF Conference on Computer Vision and Pattern Recognition*, pages 2467–2474, 2013.
- [20] Chuan Wang, Hua Zhang, Liang Yang, Si Liu, and Xiaochun Cao. Deep people counting in extremely dense crowds. In *Proceedings of the 23rd ACM International Conference on Multimedia*, pages 1299–1302, 2015.
- [21] Duc Tri Phan, Jianjun Gao, Ye Lu, Kim-Hui Yap, Kratika Garg, and Boon Siew Han. DEO-Net: Joint density estimation and object detection for crowd counting. *IEEE Transactions on Instrumentation and Measurement*, 73:1–11, 2024.
- [22] Vishwanath A Sindagi and Vishal M Patel. Generating high-quality crowd density maps using contextual pyramid cnns. In *Proceedings of the IEEE International Conference on Computer Vision*, pages 1861–1870, 2017.
- [23] Qingyu Song, Changan Wang, Yabiao Wang, Ying Tai, Chengjie Wang, Jilin Li, Jian Wu, and Jiayi Ma. To choose or to fuse? scale selection for crowd counting. In *Proceedings of the AAAI Conference on Artificial Intelligence*, volume 35, pages 2576–2583, 2021.
- [24] Mingjie Wang, Hao Cai, Xian-Feng Han, Jun Zhou, and Minglun Gong. STNet: Scale tree network with multi-level auxiliary for crowd counting. *IEEE Transactions on Multimedia*, 25:2074–2084, 2023.
- [25] Ning Liu, Yongchao Long, Changqing Zou, Qun Niu, Li Pan, and Hefeng Wu. ADCrowdNet: An attention-injective deformable convolutional network for crowd understanding. In *Proceedings of the IEEE/CVF Conference on Computer Vision and Pattern Recognition*, pages 3225–3234, 2019.
- [26] Tao Wang, Ting Zhang, Kaibing Zhang, Huake Wang, Minqi Li, and Jian Lu. Context attention fusion network for crowd counting. *Knowledge-Based Systems*, 271:110541, 2023.
- [27] Xiangyu Guo, Mingliang Gao, Guofeng Zou, Alessandro Bruno, Abdellah Chehri, and Gwanggil Jeon. Object counting via group and graph attention network. *IEEE Transactions on Neural Networks and Learning Systems*, 35(9):11884–11895, 2024.
- [28] Nicolas Carion, Francisco Massa, Gabriel Synnaeve, Nicolas Usunier, Alexander Kirillov, and Sergey Zagoruyko. End-to-end object detection with transformers. In *European Conference on Computer Vision*, pages 213–229, 2020.
- [29] Sen Lei, Zhenwei Shi, and Wenjing Mo. Transformer-based multi-stage enhancement for remote sensing image super-resolution. *IEEE Transactions on Geoscience and Remote Sensing*, 60:1–11, 2022.
- [30] Feng Tian, Sen Lei, Yingbo Zhou, Jialin Cheng, Guohao Liang, Zhengxia Zou, Heng-Chao Li, and Zhenwei Shi. Hirenet: Hierarchical-relation network for few-shot remote sensing image scene classification. *IEEE Transactions on Geoscience and Remote Sensing*, 62:1–10, 2024.
- [31] Sen Lei, Xinyu Xiao, Tianlin Zhang, Heng-Chao Li, Zhenwei Shi, and Qing Zhu. Exploring fine-grained image-text alignment for referring remote sensing image segmentation. *IEEE Transactions on Geoscience and Remote Sensing*, 63:1–11, 2025.
- [32] Ningning Lv, Min Yuan, Yufei Xie, Kun Zhan, and Fuxiang Lu. Non-local sparse attention based swin transformer v2 for image super-resolution. *Signal Processing*, 222:109542, 2024.
- [33] Jin Ning, Jie Yin, Fei Deng, and Lianbin Xie. Mabdt: Multi-scale attention boosted deformable transformer for remote sensing image dehazing. *Signal Processing*, 229:109768, 2025.
- [34] Wenhai Wang, Enze Xie, Xiang Li, Deng-Ping Fan, Kaitao Song, Ding Liang, Tong Lu, Ping Luo, and Ling Shao. Pvt v2: Improved baselines with pyramid vision transformer. *Computational Visual Media*, 8(3):415–424, 2022.
- [35] Xizhou Zhu, Weijie Su, Lewei Lu, Bin Li, Xiaogang Wang, and Jifeng Dai. Deformable detr: Deformable transformers for end-to-end object detection. *arXiv preprint arXiv:2010.04159*, 2020.
- [36] Yang Cheng and Daming Liu. AdIn-DETR: Adapting detection transformer for end-to-end real-time power line insulator defect detection. *IEEE Transactions on Instrumentation and Measurement*, 73:1–11, 2024.
- [37] Enze Xie, Wenhai Wang, Zhiding Yu, Anima Anandkumar, Jose M Alvarez, and Ping Luo. SegFormer: Simple and efficient design for semantic segmentation with transformers. *Advances in Neural Information Processing Systems*, 34:12077–12090, 2021.

- [38] Dingkan Liang, Xiwu Chen, Wei Xu, Yu Zhou, and Xiang Bai. TransCrowd: Weakly-supervised crowd counting with transformers. *Science China Information Sciences*, 65(6):160104, 2022.
- [39] Yuehai Chen, Jing Yang, Badong Chen, and Shaoyi Du. Counting varying density crowds through density guided adaptive selection cnn and transformer estimation. *IEEE Transactions on Circuits and Systems for Video Technology*, 33(3):1055–1068, 2023.
- [40] Yifei Qian, Liangfei Zhang, Xiaopeng Hong, C Donovan, Ognjen Arandjelovic, UK Fife, and PR Harbin. Segmentation assisted u-shaped multi-scale transformer for crowd counting. In *2022 British Machine Vision Conference*, page 397, 2022.
- [41] Xing Wei, Yuanrui Kang, Jihao Yang, Yunfeng Qiu, Dahu Shi, Wenming Tan, and Yihong Gong. Scene-adaptive attention network for crowd counting. *arXiv preprint arXiv:2112.15509*, 2021.
- [42] Jifeng Dai, Haozhi Qi, Yuwen Xiong, Yi Li, Guodong Zhang, Han Hu, and Yichen Wei. Deformable convolutional networks. In *Proceedings of the IEEE International Conference on Computer Vision*, pages 764–773, 2017.
- [43] Xizhou Zhu, Han Hu, Stephen Lin, and Jifeng Dai. Deformable convnets v2: More deformable, better results. In *Proceedings of the IEEE/CVF Conference on Computer Vision and Pattern Recognition*, pages 9308–9316, 2019.
- [44] Zhuofan Xia, Xuran Pan, Shiji Song, Li Erran Li, and Gao Huang. Vision transformer with deformable attention. In *Proceedings of the IEEE/CVF Conference on Computer Vision and Pattern Recognition*, pages 4794–4803, 2022.
- [45] Wenhai Wang, Jifeng Dai, Zhe Chen, Zhenhang Huang, Zhiqi Li, Xizhou Zhu, Xiaowei Hu, Tong Lu, Lewei Lu, Hongsheng Li, et al. InternImage: Exploring large-scale vision foundation models with deformable convolutions. In *Proceedings of the IEEE/CVF Conference on Computer Vision and Pattern Recognition*, pages 14408–14419, 2023.
- [46] Yaolei Qi, Yuting He, Xiaoming Qi, Yuan Zhang, and Guanyu Yang. Dynamic snake convolution based on topological geometric constraints for tubular structure segmentation. In *Proceedings of the IEEE/CVF International Conference on Computer Vision*, pages 6070–6079, 2023.
- [47] Xin Zhong, Zhaoyi Yan, Jing Qin, Wangmeng Zuo, and Weigang Lu. An improved normed-deformable convolution for crowd counting. *IEEE Signal Processing Letters*, 29:1794–1798, 2022.
- [48] Chengyang Zhang, Jie Chen, Bo Li, Min Feng, Yongquan Yang, Qikui Zhu, and Hong Bu Bu. Difference-deformable convolution with pseudo scale instance map for cell localization. *IEEE Journal of Biomedical and Health Informatics*, 28(1):355–366, 2024.
- [49] Ashish Vaswani, Noam Shazeer, Niki Parmar, Jakob Uszkoreit, Llion Jones, Aidan N Gomez, Łukasz Kaiser, and Illia Polosukhin. Attention is all you need. *Advances in Neural Information Processing Systems*, 30, 2017.
- [50] Kin Wai Lau, Lai-Man Po, and Yasar Abbas Ur Rehman. Large separable kernel attention: Rethinking the large kernel attention design in cnn. *Expert Systems with Applications*, 236:121352, 2024.
- [51] Zhaoyi Yan, Ruimao Zhang, Hongzhi Zhang, Qingfu Zhang, and Wangmeng Zuo. Crowd counting via perspective-guided fractional-dilation convolution. *IEEE Transactions on Multimedia*, 24:2633–2647, 2021.
- [52] Boyu Wang, Huidong Liu, Dimitris Samaras, and Minh Hoai Nguyen. Distribution matching for crowd counting. *Advances in Neural Information Processing Systems*, 33:1595–1607, 2020.
- [53] Yingying Zhang, Desen Zhou, Siqin Chen, Shenghua Gao, and Yi Ma. Single-image crowd counting via multi-column convolutional neural network. In *Proceedings of the IEEE/CVF Conference on Computer Vision and Pattern Recognition*, pages 589–597, 2016.
- [54] Haroon Idrees, Muhammad Tayyab, Kishan Athrey, Dong Zhang, So-maya Al-Maadeed, Nasir Rajpoot, and Mubarak Shah. Composition loss for counting, density map estimation and localization in dense crowds. In *Proceedings of the European Conference on Computer Vision*, pages 532–546, 2018.
- [55] Qi Wang, Junyu Gao, Wei Lin, and Xuelong Li. NWPU-crowd: A large-scale benchmark for crowd counting and localization. *IEEE Transactions on Pattern Analysis and Machine Intelligence*, 43(6):2141–2149, 2020.
- [56] Qingyu Song, Changan Wang, Zhengkai Jiang, Yabiao Wang, Ying Tai, Chengjie Wang, Jilin Li, Feiyue Huang, and Yang Wu. Rethinking counting and localization in crowds: A purely point-based framework. In *Proceedings of the IEEE/CVF International Conference on Computer Vision*, pages 3365–3374, 2021.
- [57] Weibo Shu, Jia Wan, Kay Chen Tan, Sam Kwong, and Antoni B Chan. Crowd counting in the frequency domain. In *Proceedings of the IEEE/CVF Conference on Computer Vision and Pattern Recognition*, pages 19618–19627, 2022.
- [58] Xinyan Liu, Guorong Li, Yuankai Qi, Zhenjun Han, Anton van den Hengel, Nicu Sebe, Ming-Hsuan Yang, and Qingming Huang. Consistency-aware anchor pyramid network for crowd localization. *IEEE Transactions on Pattern Analysis and Machine Intelligence*, pages 1–15, 2024.
- [59] Dingkan Liang, Wei Xu, and Xiang Bai. An end-to-end transformer model for crowd localization. In *European Conference on Computer Vision*, pages 38–54, 2022.
- [60] Chengxin Liu, Hao Lu, Zhiguo Cao, and Tongliang Liu. Point-query quadtree for crowd counting, localization, and more. In *Proceedings of the IEEE/CVF International Conference on Computer Vision*, pages 1676–1685, 2023.
- [61] Shengqin Jiang, Jialu Cai, Haokui Zhang, Yu Liu, and Qingshan Liu. Compare and focus: Multi-scale view aggregation for crowd counting. *IEEE Transactions on Intelligent Transportation Systems*, 25(10):13231–13239, 2024.
- [62] Zhiheng Ma, Xing Wei, Xiaopeng Hong, Hui Lin, Yunfeng Qiu, and Yihong Gong. Learning to count via unbalanced optimal transport. In *Proceedings of the AAAI Conference on Artificial Intelligence*, volume 35, pages 2319–2327, 2021.
- [63] Chenfeng Xu, Dingkan Liang, Yongchao Xu, Song Bai, Wei Zhan, Xiang Bai, and Masayoshi Tomizuka. Autoscale: Learning to scale for crowd counting. *International Journal of Computer Vision*, 130(2):405–434, 2022.